Shear Flow of an Electrically Charged Fluid by Ion Concentration Polarization: Scaling Laws for Electroconvective Vortices

Rhokyun Kwak,[1] Van Sang Pham,[2] Kian Meng Lim,[2] and Jongyoon Han[3,4,*]

[1]*Department of Mechanical Engineering, Massachusetts Institute of Technology, 77 Massachusetts Avenue, Cambridge, Massachusetts 02139, USA*

[2]*Singapore-MIT Alliance, National University of Singapore, Singapore 117576, Singapore*

[3]*Department of Electrical Engineering and Computer Science, Massachusetts Institute of Technology, 77 Massachusetts Avenue, Cambridge, Massachusetts 02139, USA*

[4]*Department of Biological Engineering, Massachusetts Institute of Technology, 77 Massachusetts Avenue, Cambridge, Massachusetts 02139, USA*

(Received 23 July 2012; published 12 March 2013)

We consider electroconvective fluid flows initiated by ion concentration polarization (ICP) under pressure-driven shear flow, a scenario often found in many electrochemical devices and systems. Combining scaling analysis, experiment, and numerical modeling, we reveal unique behaviors of ICP under shear flow: a unidirectional vortex structure, its height selection, and vortex advection. Determined by both the external pressure gradient and the electric body force, the dimensionless height of the sheared electroconvective vortex is shown to scale as $(\phi^2/U_{\mathrm{HP}})^{1/3}$, which is a clear departure from the previous diffusion-drift model prediction. To the best of our knowledge, this is the first microscopic characterization of ion concentration polarization under shear flow, and it firmly establishes electroconvection as the mechanism for an overlimiting current in realistic, large-area ion exchange membrane systems such as electrodialysis. The new scaling law has significant implications on the optimization of electrodialysis and other electrochemical systems.

DOI: 10.1103/PhysRevLett.110.114501 PACS numbers: 47.20.Ma, 47.57.jd, 47.65.Gx, 82.45.Mp

Ion exchange membranes (IEM) have been widely used for various engineering applications, such as desalination, fuel cell, biosensors, and nanofluidic devices [1–3]. In such systems, IEM acts as an "ion filter" by allowing only specific ions to pass through. This selective ion transport initiates a unique phenomenon called ion concentration polarization (ICP) near the membrane, which is characterized by significant, dynamic perturbation in ion concentrations (also known as ion depletion and ion enrichment) [1,3]. While important in many electrochemical systems, physical modeling of ICP remains challenging due to the multiphysics, multiscale nature of the problem. One of the most tantalizing problems in ICP is the mechanism of overlimiting conductance (OLC) [4], which cannot be explained by the standard theory of ICP [1] that considers only diffusion and drift. Various mechanisms for OLC have been proposed, including electroconvection (EC) (electro-osmotic instability [5–8] and bulk electroconvection [9,10]), chemical reaction (water splitting [4]), and electrostatic effects (surface conduction and electro-osmotic flow [11]). While different nonchemical mechanisms were considered important according to the scale of systems [11], the EC mechanism has been tied to OLC in macroscale systems [e.g., electrodialysis (ED)] with experimental evidences [7,8,12] and theoretical predictions [6,8] of symmetric vortex pairs. Recently, however, Andersen *et al.* [13] argued that EC may be not the source of OLC for following reasons: (i) experiments [7,8,12] were performed in microfluidic devices, and there are different sources of vortex by electrostatic effects [11] or unsymmetrical geometry (nanochannels were located only on the bottom of the channel); (ii) also, a flat depletion zone (with low concentration) is not the evidence of EC, since it can occur in microchannels without EC [14]; (iii) especially, the chemical effect "current-induced membrane discharge" could generate OLC and also suppress EC in real systems [13].

Perhaps the scientific difficulty regarding the ICP and OLC is due to the fact that there has been a general lack of direct experimental studies. Most previous studies [4,6–12,14,15] often captured ion-fluid transport behavior with 1D quiescent conductance in oversimplified systems, which cannot represent conditions of real electrochemical systems. Consequentially, they also failed to capture the effect caused by shear flow, even though many engineering systems, from conventional ED systems to new ICP devices (e.g., preconcentration [16] and desalination systems [17]) operate under shear flow in tangential direction to IEMs. While Balster *et al.* discussed the effect of flow direction on microtextured membranes, they did not go into microscopic details [18]. Recently, we developed a microscale ED system and visualized *in situ* fluid flow and ion concentration, for the purpose of investigating and optimizing the ED process [19]. In this Letter, using the micro ED platform, we investigate the concentration profile and fluid flow of ICP and verify the existence of

EC under various shear flow conditions and voltages. The experimental result is then compared with a recently developed multiscale numerical simulation [20]. In addition, a new scaling relation between the thickness of EC vortex and shear flow rate is established and validated. We also reveal the unique unidirectional vortex structure and vortex advection in sheared EC for the first time.

Figure 1 shows typical flows and ion concentration characteristics observed in the experimental system. It is noted that all parameters are controllable (e.g., flow rate, voltage, and geometry) or traceable (e.g., streamline, current, and conductivity) in the micro ED platform [19]. We also carried out multiscale numerical simulation, based on the routines developed by Pham *et al.* [20]. The simulation relies on the direct, coupled solution of the full set of Poisson-Nernst-Plank-Navier-Stokes equations (Supplemental Material [21], Fig. 1). Figure 2 shows the behavior of ion concentration polarization under shear flow: sheared EC with local ion concentrations and fluid flows, obtained from experiment and numerical simulation. The modeling results largely reproduce both flow and concentration profiles observed in the experiments, over a range of applied voltage and shear flow rates (see Supplemental Material [21], Fig. 2, for a full set of experimental data). As previously observed without shear [12], the series of wavy depletion boundary layers (thickness: d_{bl}) are generated near IEMs because EC enhances the convective mixing. However, there are unique behaviors of ICP under shear flow that have not been predicted or observed until now. These behaviors are clearly different from the traditional picture of a convective-diffusive model [1] and even from the model by Rubinstein and Zaltzman [6] where a symmetric bidirectional vortex was predicted.

The first unique behavior is that of unidirectional electroconvective vortices, in contrast with symmetric vortex pairs predicted and observed for the situation without

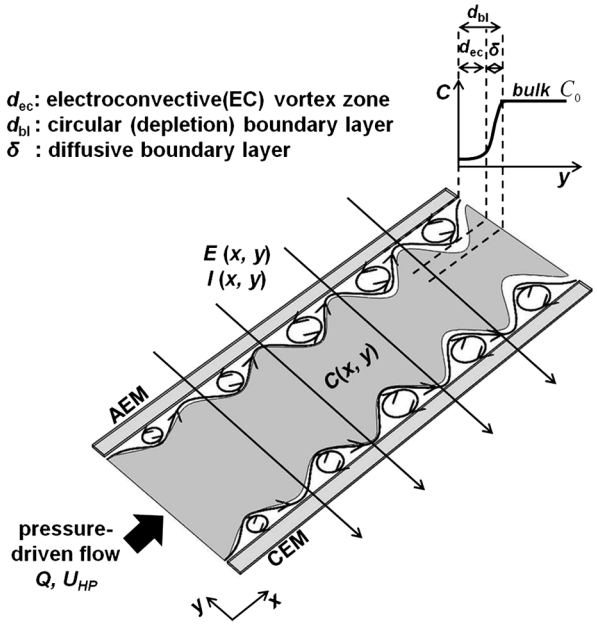

FIG. 1. Schematic diagram of sheared EC vortices (black ellipses) and ion concentration profiles C initiated by ICP under shear flow in the microscale ED system. When the pressure-driven HP flow (with flow rate Q and average velocity U_{HP}) is applied, with a sufficient high voltage V, the EC zone d_{ec} and the corresponding circular depletion boundary layer d_{bl} are observed on both CEM and AEM. The vortices have only one direction (clockwise on CEM and counterclockwise on AEM) instead of symmetric pairs. By combining the unidirectional vortices and HP flow, meandering fluid flows are induced above the EC vortices. A typical concentration profile (at the maximum height of the vortex) near the AEM, along with the thicknesses of d_{ec}, d_{bl}, and δ, are shown in the inset. C_0 indicates the bulk concentration at a given location, which gradually decreases downstream of the channel by electrodialysis [19]. The direction of electric field E and current I is from AEM to CEM (black arrows). The detailed fabrication and operating procedures are described in the Supplemental Material [21] and Kwak *et al.* [19].

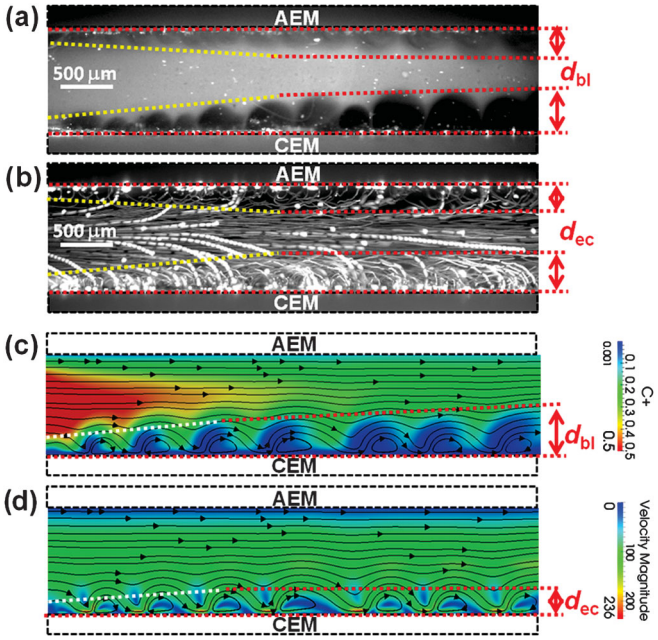

FIG. 2 (color). Sheared ICP is visualized by showing local ion concentration profiles (a) and (c) and EC vortices (b) and (d) from the experiment (at $V = 10$ V and $U_{HP} = 0.83$ mm/s ($Q = 10$ μL/min). (a) and (b) and the simulation (at $V = 25V_0$ and $U_{HP} = 80U_0$, where $V_0 = 25$ mV and $U_0 = 29.66$ μm/s; see Supplemental Material [21], Table 1) (c) and (d) CEM (AEM) is located at the bottom (top) of the channel, and the ratio of channel width to length is 1:5 in both the experiment and the simulation. In the experiment, the local ion concentration was tracked with 10 μM Rhodamine 6G (R6G), and circular depletion boundary layers d_{bl} are observed as a dark region caused by the depletion of R6G (a); in simulation, ion depletion is represented as a blue region (c). Fluid flows were visualized by stacking the time-lapse images of 10 μm polystyrene (PS) beads (b). The vortex evolution is clearly visualized at the entrance region in both the experiment and the simulation (yellow and white dotted lines).

shear flow [8,12]. When Hagen-Poiseuille (HP) flow is applied from left to right, only clockwise vortices on cation exchange membrane (CEM) and only counterclockwise vortices on anion exchange membrane (AEM) occur (Figs. 1 and 2). Unfavorably directed vortices are suppressed by the shear flow, and favorably directed vortices are expanded in the lateral direction; as a result, flow streamlines meander along the edges of these vortices. This shift from symmetric vortex pairs to asymmetric, unidirectional vortex by shear was previously observed in annular "electroconvection" in liquid crystal films [22,23]. Electroconvective vortices and corresponding ion depletion on AEM are weaker (or none in simulations) than that on CEM, due to the difference of transport properties and Stokes's radius of cation and anion (sodium and chlorine ions); the limiting currents and the overlimiting threshold voltages to generate EC are different for CEM and AEM (Supplemental Material [21], Fig. 3a) [4,24].

The second unique behavior is that of the height selection of an electroconvective vortex zone as a function of applied voltages and flow velocities. The vortex height becomes saturated, after it evolves completely at a certain distance from the entrance region of the channel (yellow and white dotted lines in Fig. 2). This reflects the fact that

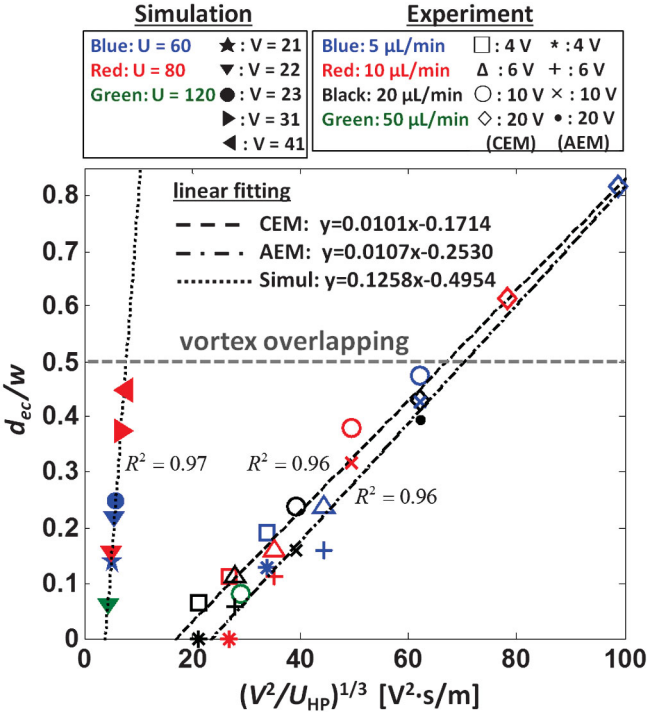

FIG. 3 (color). Dimensionless thickness of the EC vortex zone d_{ec}/w plotted against the scaling factor $(\phi^2/U_{HP})^{1/3}$ at various applied voltages and flow rates for both experiment $V = 4$–20 V and $Q = 5$–50 μL/min ($U_{HP} = 0.42$–4.17 mm/s) and simulation ($V = 21V_0$–$41V_0$ and $U_{HP} = 60U_0$–$120U_0$, where $V_0 = 25$ mV and $U_0 = 29.66$ μm/s). Dotted lines are the best fitting straight lines for two different sets of experiment data on CEM and AEM and one set of simulation data.

the vortex needs a few seconds for its evolution [12,19,25]. After this evolution, we chose the thickness of the EC vortex zone d_{ec} by a meandering streamline, which shows strong vertical motions (y direction) up to the IEMs' surfaces [black wavy streamlines in Fig. 1, red dotted lines in Figs. 2(b) and 2(d)]. This parameter largely determines the overall conductance (efficiency) of ion transport in the system. The corresponding circular depletion boundary layer d_{bl} is determined from the maximum height of regions with appreciable concentration modification from the fluorescent images [dark regions in Fig. 1, red dotted lines in Figs. 2(a) and 2(c)]; this layer includes the EC vortex zone d_{ec} and the diffusive boundary layer $\delta(\delta = d_{bl} - d_{ec})$.

The governing equations for describing ion transport across IEM are Nernst-Plank equations, Poisson's equation, and Stokes's equations (with electric body force), which represent mass transport, electrostatic balances, and viscous fluid flows [3,9]. Combining Poisson's equation and Stokes's equations, we obtain $0 = -\nabla P + \mu\nabla^2 u + \varepsilon\nabla^2\phi\nabla\phi$. Here, the first and last terms can be considered "source terms" (responsible for the viscous flow), representing the external pressure gradient and the electric body force on residual space charge, respectively (P: pressure; μ: dynamic viscosity; u: flow velocity; ε: electric permittivity; and ϕ: electric potential). If there is no external pressure gradient or shear flow, the viscous term and the electric body force term are balanced ($\mu\nabla^2 u \sim \varepsilon\nabla^2\phi\nabla\phi$). If we assume the electroconvective vortex and the electric potential drop occur only in the EC zone d_{ec} (almost all potential drop occurs within d_{ec}, due to significantly low ion concentrations (Supplemental Material [21], Fig. 6) [16,17,19]), we obtain a simple linear relation between d_{ec} and ϕ ($d_{ec} \sim \sqrt{\varepsilon/\mu\omega}\phi$, $\omega = \nabla \times u$: vorticity) as observed in previous works [7,8,12].

When HP flow is applied, however, we have to consider the external pressure gradient as well as the electroconvective flow generated from the membrane walls. The tangential flow is developed by the external pressure gradient, and the vortical flow is developed by the electric body force. At the boundary of the EC zone d_{ec}, therefore, these two driving forces will be balanced: $\nabla P \sim \varepsilon\nabla^2\phi\nabla\phi$. The pressure gradient can be described with the average flow velocity of HP flow U_{HP}, the hydrodynamic diameter of the channel D_h, $P/L \sim 64\mu U_{HP}/D_h^2$, and $D_h = 2wh/(w + h)$ for rectangular channels (L: length; w: width; h: height) [26]. As a result, we obtain a scaling relation for sheared EC,

$$\frac{d_{ec}}{w} \sim C\left(\frac{\phi^2}{U_{HP}}\right)^{1/3}, \qquad C = \left[\frac{\varepsilon}{64\mu w^3}\left(\frac{2wh}{w+h}\right)^2\right]^{1/3}. \quad (1)$$

This scaling relation, which is clearly different from conventional convective-diffusive model $(d_{bl}/w)^3 \sim (D/U_{HP}w)(x/w)$ (D: diffusivity of ions) (Eq. 6.2.12 in Ref. [1]), reveals that the dimensionless thickness of the EC zone d_{ec}/w is linearly proportional to $(\phi^2/U_{HP})^{1/3}$.

The scaling constant C, predicted from structural parameters of the channel, is 0.0107 and 0.1303 for the experimental system ($w = 1$ mm, $h = 0.2$ mm) and simulation ($w = 20$ μm, $h \to \infty$), respectively ($\mu = 0.001$ kg/m · s, $\varepsilon = 80 \times 8.854 \times 10^{-12}$ F/m). Figure 3 shows the dimensionless thickness of the EC zone for various experimental and simulation conditions according to the scaling factor $(\phi^2/U_{\mathrm{HP}})^{1/3}$. Not only do all measured values collapse onto straight lines (dotted lines in Fig. 3) but also the slopes of the lines (experiment: 0.0101/0.0107 on CEM and AEM; simulation: 0.1258) agree well with the scaling constant (error <5%). These fitting lines do not pass through the origin, because the onset of EC instability occurs at the finite voltage (Supplemental Material [21], Fig. 2). It is noted that the overlimiting threshold voltage is fixed even under different flow rates (Supplemental Material [21], Fig. 4).

This scaling analysis allows one to predict ion concentrations and fluid flows by sheared ICP, which routinely occurs in real electrochemical systems. At low voltage or strong HP flow, $(\phi^2/U_{\mathrm{HP}})^{1/3} \ll 1$ ($\nabla P \gg \varepsilon \nabla^2 \phi \nabla \phi$), the thickness of the EC zone d_{ec}/w is near zero. The EC is completely suppressed or flushed away by HP flow, so tangential flow patterns largely dominate in the system, with a minimal diffusion layer near the IEMs (Supplemental Material [21], Fig. 5). As the scaling factor $(\phi^2/U_{\mathrm{HP}})^{1/3}$ increases, the region governed by the EC expands and the sheared EC zone begins to appear, along with circular depletion boundary layers and meandering flow patterns. When d_{ec}/w becomes larger than 0.5, the vortices on CEM and AEM start to overlap and interact with each other, inducing strongly chaotic behaviors both for ion concentration and fluid flows. The concentration or flow profiles from simulation and experiment are well matched when d_{ec}/w is similar, even when other parameters (e.g., Reynolds number and other structural dimensions) are not equal (Supplemental Material [21], Fig. 4). This would indicate that the balance of HP and EC flows primarily governs the concentration or flow profiles of the system. In this experiment and simulation, diffusion is suppressed by fast HP flow. Therefore, the diffusive boundary layers δ do not increase significantly (Supplemental Material, Fig. 5).

The last unique behavior is that of vortex advection along the direction of the shear flow (Fig. 4) (see Supplemental Material videos [21]). As described in previous studies without shear, the vortex width and height are determined by the applied voltage as well as the geometry of the system [6,8,12], but the position of the vortex is not fixed and can be shifted. Under tangential shear flow, EC vortices would migrate. The vortex advection speed (U_{ec}) only depends on the average flow velocity and is largely independent of the applied voltage (Supplemental Material [21], Fig. 7). This is the case for both experimental and simulation results. As all existing vortices advect downstream, new vortices are generated at the front end of the channel; therefore, the overall concentration or flow profiles are maintained, except for the temporal or spatial fluctuation [Fig. 4(a)].

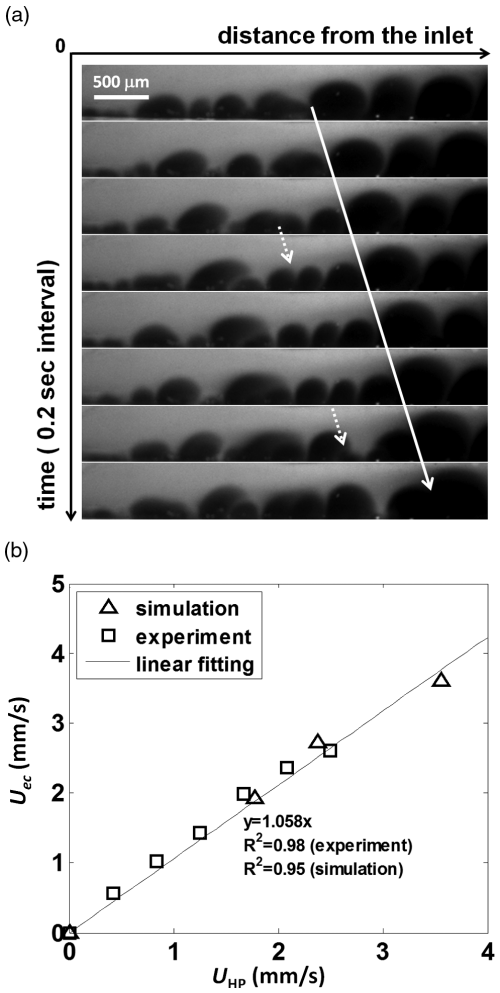

FIG. 4. (a) Space-time plot of vortex advection visualized by the corresponding circular depletion boundary layer. The time interval between adjacent images is 0.2 s. Even when neighboring vortices merge or separate (white dotted arrows), their advection with constant speed is clearly observed (white solid arrow). (b) Vortex advection speed U_{ec} according to the average flow velocity U_{HP} rectangle: experiments at $U_{\mathrm{HP}} = 0.42$–2.5 mm/s ($Q = 5$–30 μL/min); triangle: simulations at $U_{\mathrm{HP}} = 1.78$–3.56 mm/s ($U_{\mathrm{HP}} = 60U_0$–$120U_0$, $U_0 = 29.66$ μm/s). The best fitting curves for both experiment and simulation results are the same, $y = 1.058x$ (the x intercept is set at 0).

Our experiments and modeling results reveal significant insights regarding the physics of ion concentration polarization. Contrary to recent hypothesis [13], it firmly establishes that electroconvective vortices do occur in realistic systems, largely determining the boundary layer and ion transport efficiency. The flow and concentration patterns observed in this work are not compatible with any other proposed mechanisms of OLC [4,11,13] except electroconvection [6]. We validate this by reproducing

the observed experimental behaviors with *ab initio*, multiscale numerical modeling of the system. In addition, we reveal the new scaling law that governs the thickness of electroconvective vortex under shear flow. This new relation is a clear departure from the previous characterization [1,7,8,12] and therefore has significant implications in optimizing many electrochemical systems.

This work was supported by the NSF (CBET-0854026) and DARPA Cipher program, as well as the Singapore-MIT Alliance II, CE programme. R. K. was partially supported by Kwanjeong Educational Foundation, Korea. We appreciate Guofeng Guan, Yongxue Huang, and Weng Kung Peng (SMART Centre, BioSyM IRG, Singapore) for their support of the device fabrication.

*Corresponding author.
jyhan@mit.edu

[1] R. F. Probstein, *Physicochemical Hydrodynamics: An Introduction* (Wiley-Interscience, New York, 2003), 2nd ed.
[2] C. R. Martin and Z. S. Siwy, Science **317**, 331 (2007).
[3] S. J. Kim, Y. A. Song, and J. Han, Chem. Soc. Rev. **39**, 912 (2010).
[4] V. V. Nikonenko, N. D. Pismenskaya, E. I. Belova, P. Sistat, P. Huguet, G. Pourcelly, and C. Larchet, Adv. Colloid Interface Sci. **160**, 101 (2010).
[5] I. Rubinstein, E. Staude, and O. Kedem, Desalination **69**, 101 (1988).
[6] I. Rubinstein and B. Zaltzman, Phys. Rev. E **62**, 2238 (2000).
[7] S. J. Kim, Y. C. Wang, J. H. Lee, H. Jang, and J. Han, Phys. Rev. Lett. **99**, 044501 (2007).
[8] S. M. Rubinstein, G. Manukyan, A. Staicu, I. Rubinstein, B. Zaltzman, R. G. H. Lammertink, F. Mugele, and M. Wessling, Phys. Rev. Lett. **101**, 236101 (2008).
[9] I. Rubinstein, Phys. Fluids A **3**, 2301 (1991).
[10] T. Pundik, I. Rubinstein, and B. Zaltzman, Phys. Rev. E **72**, 061502 (2005).
[11] E. V. Dydek, B. Zaltzman, I. Rubinstein, D. S. Deng, A. Mani, and M. Z. Bazant, Phys. Rev. Lett. **107**, 118301 (2011).
[12] G. Yossifon and H. C. Chang, Phys. Rev. Lett. **101**, 254501 (2008).
[13] M. B. Andersen, M. van Soestbergen, A. Mani, H. Bruus, P. M. Biesheuvel, and M. Z. Bazant, Phys. Rev. Lett. **109**, 108301(2012).
[14] A. Mani and M. Bazant, Phys. Rev. E **84**, 061504 (2011).
[15] I. Rubinstein and B. Zaltzman, Adv. Colloid Interface Sci. **159**, 117 (2010).
[16] R. Kwak, S. J. Kim, and J. Han, Anal. Chem. **83**, 7348 (2011).
[17] S. J. Kim, S. H. Ko, K. H. Kang, and J. Han, Nat. Nanotechnol. **5**, 297 (2010).
[18] J. Balster, M. H. Yildirim, D. F. Stamatialis, R. Ibanez, R. G. Lammertink, V. Jordan, and M. Wessling, J. Phys. Chem. B **111**, 2152 (2007).
[19] R. Kwak, G. Guan, W. K. Peng, and J. Han, Desalination **308**, 138 (2013).
[20] V. S. Pham, Z. Li, K. M. Lim, J. K. White, and J. Han, Phys. Rev. E **86**, 046310 (2012).
[21] See Supplemental Material at http://link.aps.org/supplemental/10.1103/PhysRevLett.110.114501 for experimental setup, simulation details, and extensive analysis regarding the scaling laws.
[22] Z. A. Daya, V. B. Deyirmenjian, S. W. Morris, and J. R. de Bruyn, Phys. Rev. Lett. **80**, 964 (1998).
[23] Z. A. Daya, V. B. Deyirmenjian, and S. W. Morris, Phys. Fluids **11**, 3613 (1999).
[24] N. P. Berezina, N. A. Kononenko, O. A. Dyomina, and N. P. Gnusin, Adv. Colloid Interface Sci. **139**, 3 (2008).
[25] E. A. Demekhin, V. S. Shelistov, and S. V. Polyanskikh, Phys. Rev. E **84**, 036318 (2011).
[26] F. M. White, *Fluid Mechanics* (McGraw-Hill, New York, 2003), 5th ed.